ACS PHYSICAL CHEMISTRY Au
AN OPEN ACCESS JOURNAL OF THE AMERICAN CHEMICAL SOCIETY

pubs.acs.org/physchemau

Article

Unsymmetric Pentacene- and Pentacenequinone-Fused Porphyrins: Understanding the Effect of Cross- and Linear-Conjugation

Austen Moss,[†] Dustin E. Nevonen,[†] Yi Hu, Vladimir N. Nesterov, Victor N. Nemykin,* and Hong Wang*

Cite This: *ACS Phys. Chem Au* 2022, 2, 468–481

Read Online

ACCESS | Metrics & More | Article Recommendations | Supporting Information

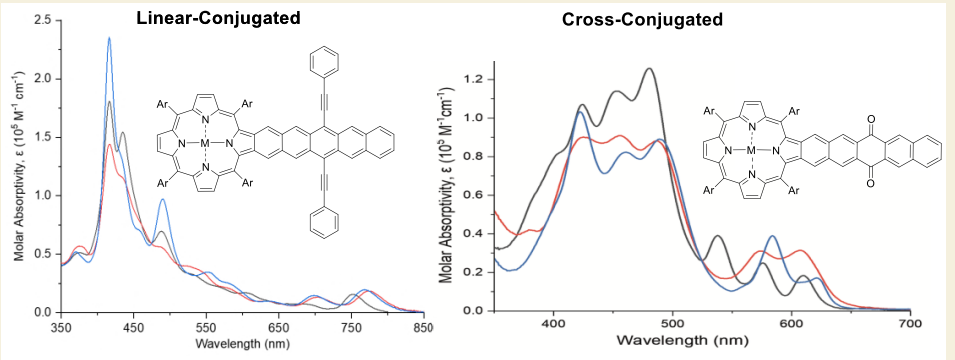

ABSTRACT: Unsymmetric pentacenequinone-fused (cross-conjugated) and pentacene-fused (linear-conjugated) porphyrins were designed and synthesized. The cross-conjugated ($\mathbf{AM_1}$−$\mathbf{AM_3}$) and linear-conjugated ($\mathbf{AM_5}$−$\mathbf{AM_7}$) porphyrins displayed strikingly different sets of optical and electronic properties, both of which are unusual and nontypical of porphyrins. MCD, DFT, and TDDFT calculations suggest that multiple charge transfer states exist in both π-conjugated systems, which contributes to the complex absorption and MCD spectra of these molecular systems. The general Gouterman's four-orbital model used to explain porphyrin spectroscopy led to contradicting theoretical and experimental data, and is thus not applicable for these molecular systems. The "2 + 4" and "3 + 3" active spaces have been deduced and have proven effective to interpret the absorption and MCD spectra of the pentacenequinone-fused (cross-conjugated) and pentacene-fused (linear-conjugated) porphyrins, respectively. Spectroelectrochemistry of $\mathbf{AM_5}$−$\mathbf{AM_7}$ revealed broad and intense IR absorptions in the range of 1500−2500 nm, illustrating the exceptional ability of these pentacene-fused systems to accommodate positive charges. A pronounced metal effect was observed for pentacene-fused porphyrins. While pentacene-fused Ni(II) porphyrin ($\mathbf{AM_6}$) demonstrated an abnormal ability to stabilize pentacene with a half-life of >28.3 days, the half-life of the free base and Zn(II) counterparts were normal, similar to those of pentacene analogues. This work provides important and useful information on guiding new material designs.

KEYWORDS: *pentacene, cross- and linear-conjugation, MCD spectroscopy, π-extended porphyrin, TDDFT calculation, UV−vis spectroscopy, cyclic voltammetry*

INTRODUCTION

π-Extended structures have received intense attention due to their relevance in various topics in chemistry, physics, and materials science.[1,2] π-Extended porphyrins fused with polycyclic aromatic hydrocarbons (PAHs) are especially attractive as they are reminiscent of "nanographenes" doped with heteroatoms. π-Extended porphyrins possess a unique combination of photophysical, optoelectronic, and physicochemical properties, which are of broad interest in various areas ranging from biomedicine to organic electronics.[3−12] π-Extended porphyrins can be classified into two categories: *meso*, *β*-fused and *β*, *β*-fused. Although synthetically challenging, both *meso*, *β*-PAH-fused and *β*, *β*-PAH-fused porphyrins have been successfully achieved (Figure 1).[3−39] These π-extended structures display remarkable electronic and optical properties, which have never been reported for other molecular systems.

Our group has been engaged in developing synthetic methods to fuse larger PAHs at porphyrin *β*, *β*-positions.[40−45] *β*, *β*-Fusion offers a unique geometry and topology for PAHs not accessible through *meso*, *β*-fusion, opening new doors to

Received: May 25, 2022
Revised: July 12, 2022
Accepted: July 12, 2022
Published: July 29, 2022

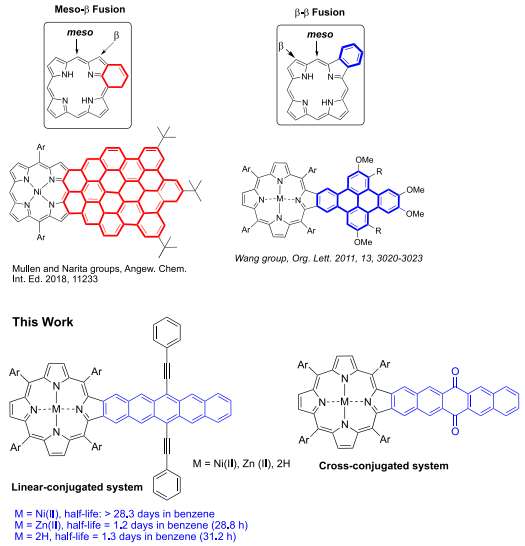

Figure 1. Selected examples of large PAH-fused porphyrins.

construct π-extended systems in materials science. In a previous publication, we prepared pentacenequinone- and pentacene-fused porphyrin dimers.[43] Despite their similar D_{2h} symmetry, the pentacenequinone- and pentacene-fused porphyrin dimers displayed strikingly different electronic and optical properties, both of which are unprecedented and very interesting. In particular, the pentacene-fused nickel porphyrin dimer exhibited abnormally high stability, which was >60 times more stable than that of the corresponding pentacene.[43]

The unusual properties of these pentacenequinone- and pentacene-fused porphyrin dimers prompted us to investigate the underlying factors governing the observed redox and optical behaviors. The first questions to be answered are the following: Will other pentacenequinone- and pentacene-fused porphyrins display similar properties? How does cross-conjugation (pentacenequinone-fused) and linear-conjugation (pentacene-fused) perturb the spectroscopy differently? Importantly, stability issues have been one major challenge for longer acenes to overcome. Will fusion of Ni(II) porphyrin to acenes potentially become an effective strategy to tackle this challenge? Cross-conjugated chromophoric systems have been rarely investigated.[46,47] Through answering these questions, we hope to provide information on new principles for materials design.

In this work, we introduce a new series of monopentacenequinone- and monopentacene-fused porphyrins (Figure 1), which possess an effective C_{2v} symmetry in comparison with their dimer analogues of D_{2h} symmetry.[43] Studies on these π-extended structures using UV−vis and florescence spectroscopies, cyclic voltammetry (CV), and spectroelectrochemistry reveal unprecedented optical and electronic properties, which sharply contrast their dimer analogues.[43] Magnetic circular dichroism (MCD) spectroscopy, DFT and TDDFT calculations were carried out to understand the electronic transitions of these compounds as well as the correlations between cross-conjugated and linear-conjugated systems. In this work, Zn(II)-, 2H-, and Ni(II)-pentacene-fused porphyrins have also been made available to investigate the center metal effect on the stability of the pentacenes.

RESULTS AND DISCUSSION

Molecular Design and Synthesis

In the previous work,[43] we showed that the pentacene-fused nickel porphyrin dimer exhibited abnormally high stability. This exceptional stability was mainly attributed to the presence of the nickel ion.[43] Attempts to use a Zn(II) pentacenequinone-fused porphyrin dimer to prepare the corresponding Zn(II) pentacene-fused porphyrin dimer did not succeed. We suspected that zinc could easily be demetalated upon addition of the phenyl acetylide to the quinone due to ring deformation and the resulting free-base porphyrin would be deprotonated by the strongly basic phenyl acetylide. Since there are two porphyrins fused to the pentacenequinone, the presence of two negatively charged porphyrins could effectively deactivate the quinone group toward an addition reaction. In the monopentacenequinone- and monopentacene-fused porphyrins, the presence of only one porphyrin will relieve the steric hindrance and thus alleviate the deformation of the porphyrin ring during the addition reaction. In addition, it is hopeful that the addition reaction to quinone would not be fully deactivated with one negatively charged porphyrin.

The synthesis of monopentacenequinone-fused (**AM$_1$**−**AM$_3$**) and monopentacene-fused porphyrins (**AM$_5$**−**AM$_7$**) started with monobenzoporphyrin dicarbaldehyde **1**, which was prepared using a previously reported procedure. Monobenzoporphyrin **1**, cyclohexane-1,4-dione, and benzene-1,2-dicarbaldehyde were mixed in THF under basic condition (KOH/MeOH) to give the desired monopentacenequinone-fused porphyrin **AM$_1$** in an 84% yield (Scheme 1). Different

Scheme 1. Synthesis of Unsymmetrical Pentacenequinone-Fused Porphyrins

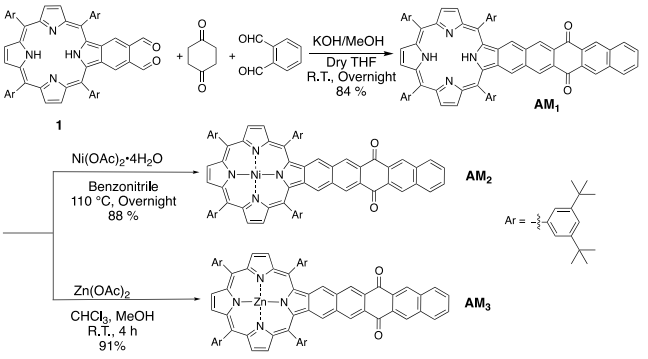

ratios of **1**, cyclohexane-1,4-dione, and benzene-1,2-dicarbaldehyde were attempted, and the best yield was achieved with a molar ratio of 1:20:40. Monopentacenequinone-fused porphyrins **AM$_2$** and **AM$_3$** were obtained through insertion of Ni(II) and Zn(II), respectively.

The synthesis of the pentacene-fused porphyrins followed previously reported protocols (Scheme 2).[42,43] The addition of phenyl acetylene to **AM$_1$** was accomplished by adding phenyl acetylide, produced from the reaction of phenyl acetylene with *n*-butyl lithium in THF at −78 °C, to a solution of **AM$_1$** in THF under argon atmosphere to form the double addition product **AM$_4$-2H** in 72% yield. Reduction of **AM$_4$-2H** using $SnCl_2$ gave **AM$_5$** in 93% yield. **AM$_6$** was obtained in a similar manner starting with **AM$_2$**. The addition product **AM$_4$-Ni** was also isolated. The zinc analogue **AM$_7$** was prepared through the

https://doi.org/10.1021/acsphyschemau.2c00023
ACS Phys. Chem Au 2022, 2, 468−481

Scheme 2. Synthesis of Unsymmetrical Pentacene-Fused Porphyrins

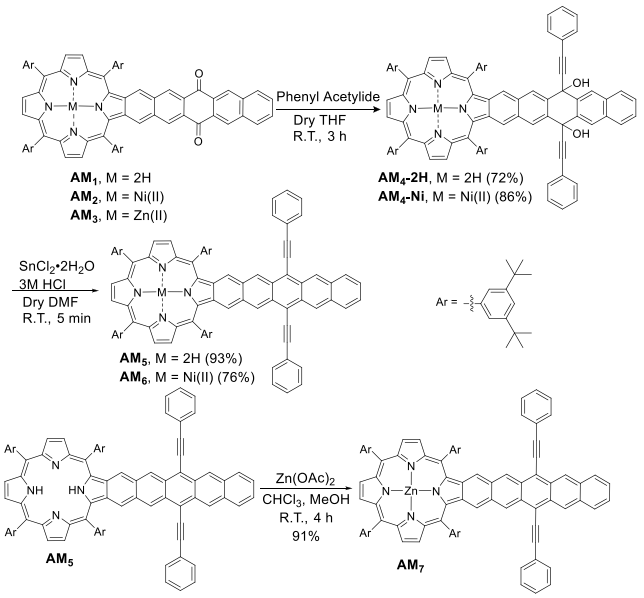

insertion of Zn(II) into free base $\mathbf{AM_5}$ under argon atmosphere.

X-ray Crystallography

Single crystals suitable for X-ray analysis were obtained for $\mathbf{AM_1}$ (CCDC, 2080553), $\mathbf{AM_2}$ (CCDC, 2080554), and $\mathbf{AM_3}$ (CCDC, 2080555) through vapor diffusion (Figure 2 and

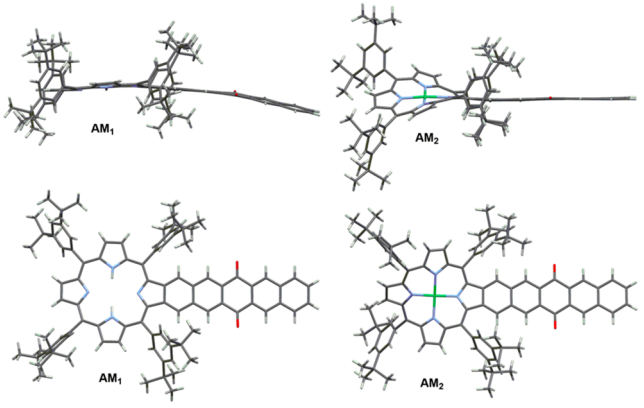

Figure 2. X-ray crystal structure of $\mathbf{AM_1}$ and $\mathbf{AM_2}$. All hydrogen atoms are omitted for clarity.

Figure S1 in the Supporting Information (SI)). Both the pentacenequinone component and the porphyrin core of free base $\mathbf{AM_1}$ adopt essentially a planar conformation with the porphyrin core slightly saddled and the pentacenequinone slightly curved. The pentacenequinone component and the porphyrin core are also aligned in the same plane. In contrast, while the pentacenequinone component remains planar, the porphyrin core of Ni(II) $\mathbf{AM_2}$ is significantly distorted from planarity, assuming a ruffled conformation. Although the X-ray crystal data obtained for Zn(II) $\mathbf{AM_3}$ is of low quality, the core structures can be clearly distinguished (see Figure S1 in the SI). Similar to its free-base analogue $\mathbf{AM_1}$, both the pentacenequinone component and the porphyrin core of $\mathbf{AM_3}$ are essentially planar with the pentacenequinone slightly twisted at the center cyclohexane-1,4-dione ring. The pentacenequinone plane and the porphyrin plane of $\mathbf{AM_3}$ are also slightly twisted from each other.

It is notable that significant $\pi-\pi$ type stacking is observed for $\mathbf{AM_1}$ (Figure 3). Two $\mathbf{AM_1}$ molecules are lying on the top

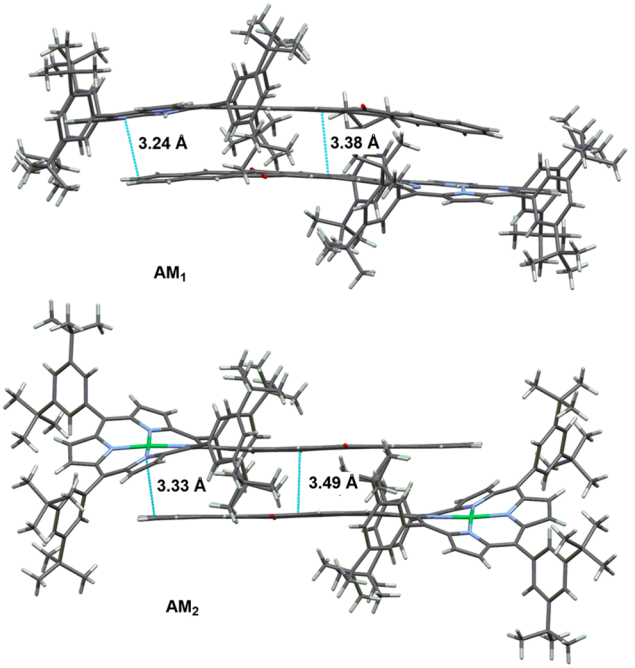

Figure 3. Crystal packing of $\mathbf{AM_1}$ and $\mathbf{AM_2}$. All hydrogen atoms are omitted for clarity.

of each other through the pentacenequinone components with a distance of 3.24−3.38 Å, which fits well in the distance range for $\pi-\pi$ stacking. The two porphyrin rings are at the opposite side of each other. The stacking is not entirely cofacial and is slightly slipped. Despite the largely distorted porphyrin ring, $\mathbf{AM_2}$ shows similar packing in the solid state with a slightly longer packing distance (3.33−3.49 Å). These data suggest that the pentacenequinone component can exert relatively strong $\pi-\pi$ interactions.

UV-Vis and Fluorescence Spectroscopy

The UV−vis absorption spectra of pentacenequinone-fused porphyrins $\mathbf{AM_1}$−$\mathbf{AM_3}$ and pentacene-fused porphyrins $\mathbf{AM_5}$−$\mathbf{AM_7}$ are compiled in Figures 4 and 5, respectively. All three monoporphyrin-fused pentacenequinones $\mathbf{AM_1}$−$\mathbf{AM_3}$ displayed three prominent bands in the Soret band region spanning from ∼320 to ∼550 nm. The intensities of these transitions are almost even, which is in sharp contrast to those of their pentacenequinone-fused porphyrin dimers showing nontypical porphyrin absorptions. This unusual splitting pattern has never been observed in any other porphyrins to our knowledge.[48] It is interesting to note that when phenylacetylide was added to the quinone groups of $\mathbf{AM_1}$ and $\mathbf{AM_2}$, the absorption bands of the resulting porphyrins ($\mathbf{AM_4}$-**2H** and $\mathbf{AM_4}$-**Ni**) showed typical porphyrin absorptions with one sharp Soret band and several weaker Q bands. It is apparent that the abnormal spitting pattern observed for the Soret bands of $\mathbf{AM_1}$−$\mathbf{AM_3}$ can be mainly attributed to the cross-conjugation in $\mathbf{AM_1}$−$\mathbf{AM_3}$. Linear-conjugated pentacene-fused porphyrins $\mathbf{AM_5}$−$\mathbf{AM_7}$ showed complex features of the Soret bands which is not uncommon for porphyrins with

https://doi.org/10.1021/acsphyschemau.2c00023
ACS Phys. Chem Au 2022, 2, 468−481

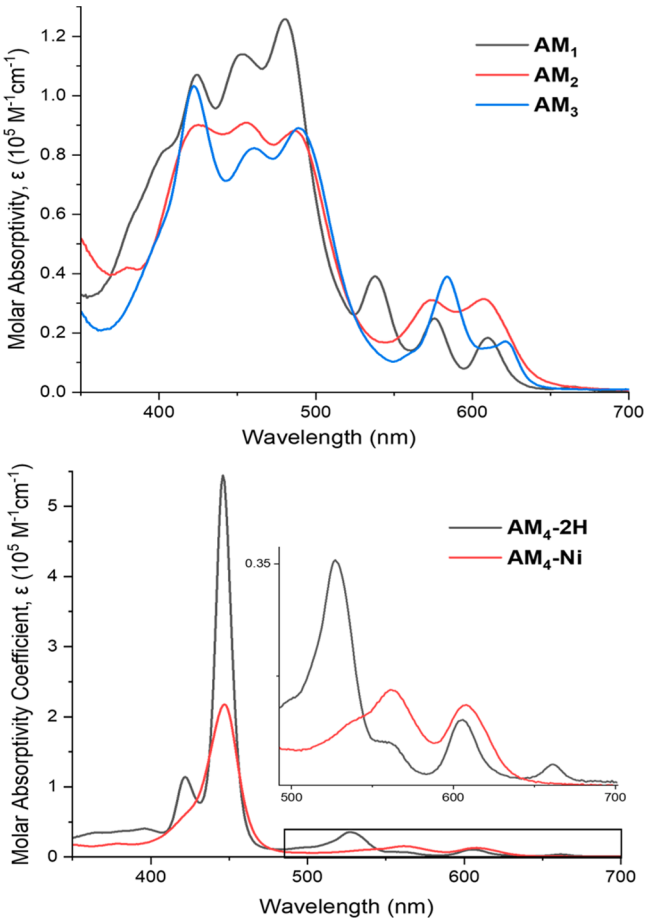

Figure 4. UV−vis absorption spectra of AM_1−AM_3, AM_4-Ni, and AM_4-2H in DCM. Inset: Expanded region for Q bands.

reduced symmetry. Additionally, the electronic interaction between the porphyrin and pentacene causes absorptions spanning across most of the visible portion and into the near-infrared (AM_5: λ_{max} = 753 nm, AM_6: λ_{max}= 773 nm, AM_7: λ_{max} = 770 nm) region of the electromagnetic spectrum, which is expected for π-extended systems. On the other hand, AM_5−AM_7 exhibited excessive absorption peaks compared toa normal π-extended porphyrin possessing C_{2v} symmetry,[3−12,26] suggesting the existence of complex electronic events in the molecular system. The sharp contrast in the absorption spectra between the cross-conjugated system and the linear-conjugated system reflects different effects of electronic perturbations on the optical properties of these two molecular systems. Further investigation of the electronic transitions present in these molecules was necessary to better understand their optical properties.

Steady state fluorescence spectra of AM_1, AM_3, AM_5, and AM_7 were measured in benzene (Figure S2 in the SI). Both pencenequinone-fused porphyrins AM_1 and AM_3 exhibited two strong emission bands with similar intensities in the range of 550−800 nm. Both emission bands of free base-porphyrin AM_1 are red-shifted by ∼42 nm as compared with those of Zn(II) porphyrin AM_3. Pentacene-fused porphyrins AM_5 and AM_7 only showed one major emission band at 767 and 790 nm with a weak and broad shoulder peak centered at 850 and 871 nm, respectively. Interestingly, in contrast to the cross-conjugated AM_1 and AM_3 where free-base porphyrin AM_1 exhibited red-shifted emission bands relative to those of Zn(II)

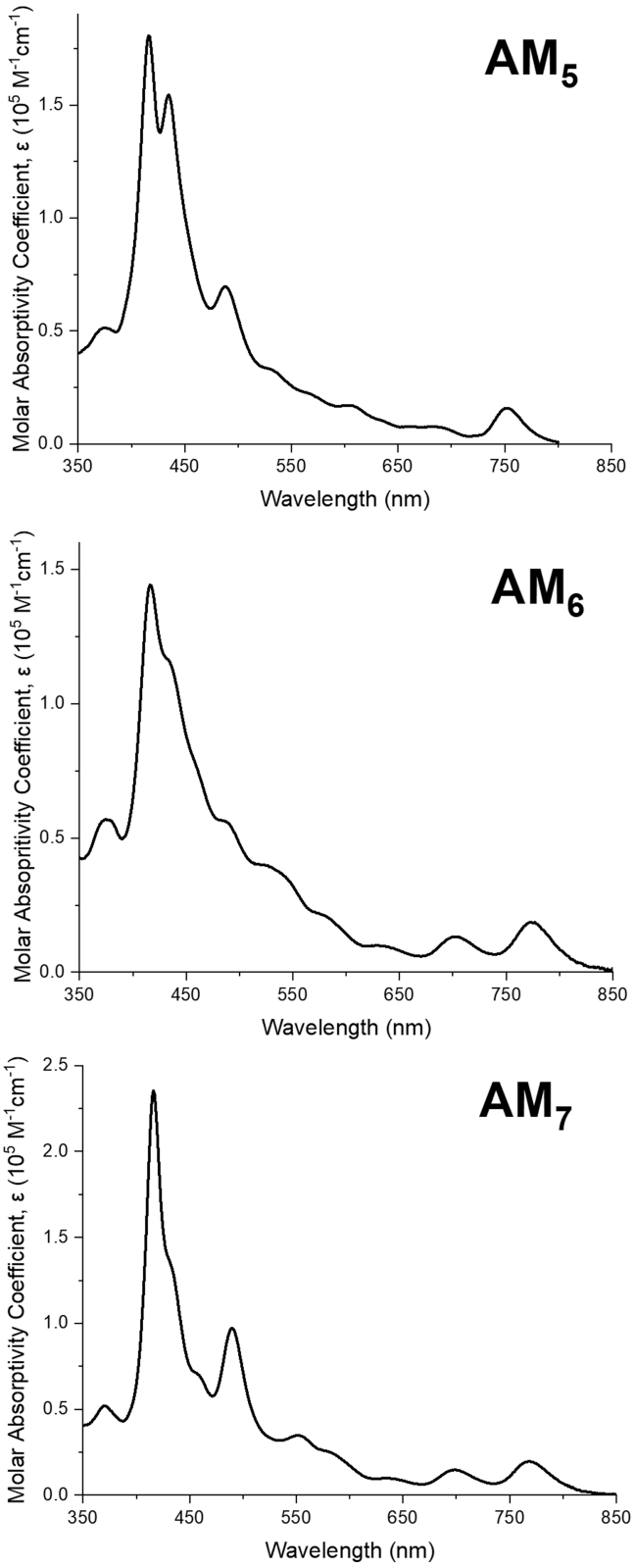

Figure 5. UV−vis/NIR absorption spectra of AM_5−AM_7 in DCM.

porphyrin AM_3, linear-conjugated Zn(II) porphyrin AM_7 showed a more red-shifted emission band than those of free-based porphyrin AM_5. Ni(II) porphyrins AM_2 and AM_6 were nonfluorescent. The fluorescence of pentacene and pentacenequinone was obviously quenched by the fused nickel porphyrin. The optical data of these porphyrins are organized

https://doi.org/10.1021/acsphyschemau.2c00023
ACS Phys. Chem Au 2022, 2, 468−481

in Table 1. The optical HOMO−LUMO gaps are in the order of **AM$_6$** (1.65 eV) < **AM$_7$** (1.66 eV) < **AM$_5$** (1.69 eV) < **AM$_1$** (1.89 eV) < **AM$_3$** (2.02 eV) < **AM$_2$** (2.07 eV).

Table 1. Redox Potentials of the Studied Compounds

samples	redox potential, V (FcH/FcH$^+$)	
	E_{ox}	E_{red}
AM$_1$	0.54; 0.62; 1.01	−2.19; −2.09; −1.84; −1.65
AM$_2$	0.43; 0.60	−1.98; −1.75; −1.60
AM$_3$	0.22; 0.42; 0.71; 0.95	−1.97; −1.67; −1.31
AM$_5$	0.19; 0.64; 1.04; 1.49	−1.81; −1.44
AM$_6$	0.14; 0.45; 0.62; 0.97; 1.26	−2.11; −1.83; −1.75; −1.39
AM$_7$	0.08; 0.36; 0.61; 0.93; 1.08; 1.36	−1.85; −1.45

MCD Spectroscopy

Magnetic circular dichroism (MCD) spectroscopy was utilized to understand the unusual splitting pattern of the absorption bands of **AM$_1$**−**AM$_7$**. The UV−vis and MCD spectra of porphyrins **AM$_1$**−**AM$_3$** and **AM$_5$**−**AM$_7$** are shown in Figures 6 and 7. In the case of metal-free **AM$_1$**, four MCD Faraday *B*-terms were observed at 666, 616, 580, and 549 nm in the Q-band region. The two lower energy bands have negative amplitudes, and the two higher energy bands have positive amplitudes. These transitions correlate well with the absorption bands at 664, 610, 575, and 537 nm observed in the UV−vis spectrum of this compound. In the Soret band region, the most intense transitions at 480, 453, and 423 nm observed in the UV−vis spectrum of **AM$_1$** correlate well with the negative MCD transition at 474 nm, the negative amplitude shoulder at 450 nm, and the positive amplitude *B*-term at 423 nm. In addition, a MCD pseudo-*A*-term was observed between 392 and 376 nm (Figure 6). The Q-band region in the transition-metal complexes **AM$_2$** and **AM$_3$** differs substantially from metal-free **AM$_1$**. Indeed, in both cases, a pair of the MCD pseudo-*A*-terms was observed in the Q-band region, with the lower energy pseudo-*A*-term being about two times more intense compared to the higher energy one (Figure 6). Such behavior (the presence of two MCD pseudo-*A*-terms in the Q-band region) has been observed in the case of bimetallic pentacenequinone-fused porphyrins published by us.[42] Moreover, the energies of the main transitions observed in the Q-band region of the porphyrins **AM$_2$** and **AM$_3$** are very close to those reported for their doubly fused analogues.[42] This observation suggests the similarity of the HOMO−LUMO gap in mononuclear porphyrins **AM$_2$** and **AM$_3$** and the binuclear analogue, which might indicate the, at least partial, π-system interruption in the later compounds caused by the pentacenequinone bridge. The MCD signatures of porphyrins **AM$_2$** and **AM$_3$** in the Soret band region resemble those for the metal-free **AM$_1$**. In particular, two lower energy bands in the UV−vis spectra of **AM$_2$** (486 and 456 nm) and **AM$_3$** (489 and 460 nm) are associated with two *B*-terms of negative amplitude, while the intense higher energy band (424 nm for **AM$_2$** and 422 nm for **AM$_3$**) is associated with the positive amplitude *B*-term in their MCD spectra. In addition, an MCD pseudo-*A*-term was observed for both transition-metal compounds between 395 and 369 nm. It is expected that the elongation of the porphyrin conjugation using the pentaquinone substituent will significantly increase the energy difference between Gouterman's pair of $e_g(x)$ and $e_g(y)$ orbitals (in traditional D_{4h} point group notation).[49,50] The MCD spectra in

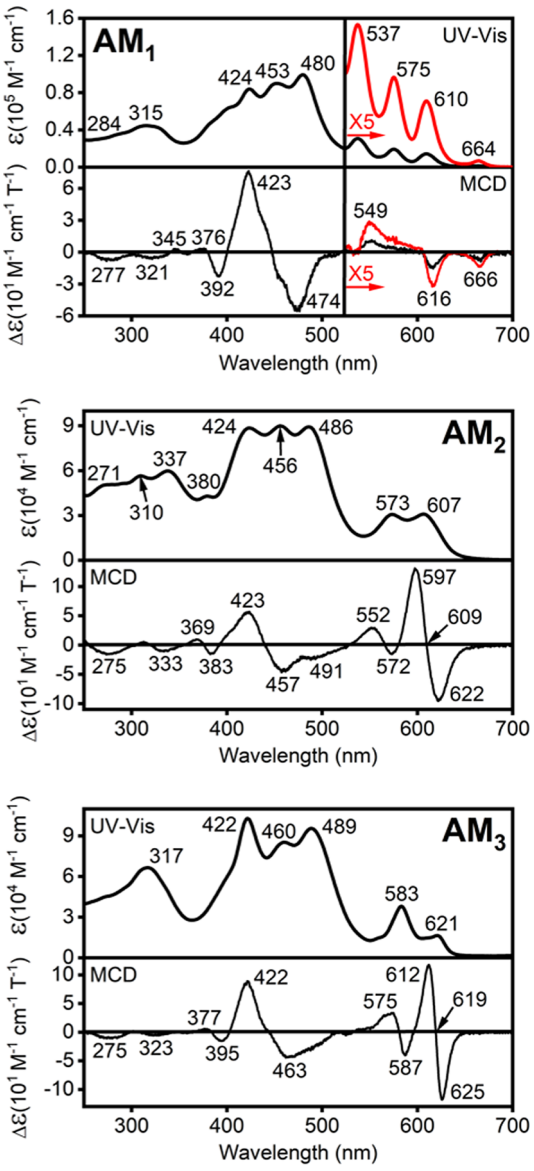

Figure 6. UV−vis and MCD spectra of porphyrins **AM$_1$**−**AM$_3$** in DCM.

the Q-band region, however, have a negative-to-positive amplitude sequence (in ascending energy), which is indicative of the ΔHOMO > ΔLUMO relationship (ΔHOMO is the energy difference between the a_{1u} and a_{2u} MOs in Gouterman's notation, and ΔLUMO is the energy difference between the $e_g(x)$ and $e_g(y)$ MOs in Gouterman's notation).[51−55]

The Q-band region in the pentacene-fused porphyrins **AM$_5$**−**AM$_7$** is significantly more red-shifted compared to that in the pentacenequinone-fused porphyrins **AM$_1$**−**AM$_3$** (Figure 7). For instance, the lowest energy transition in all compounds was observed between 755 and 781 nm. This band is associated with a very weak MCD *B*-term with a negative amplitude. The energy of this weak MCD *B*-term correlates well with the position of the lowest energy transition observed in the UV−vis spectra of **AM$_5$**−**AM$_7$**. The next MCD signal belongs to the pseudo-*A*-term centered around 690−705 nm. Unlike in the case of the pentacenequinone-fused systems **AM$_1$**−**AM$_3$**, the pseudo-*A*-term was observed for the metal-free and transition-metal complexes **AM$_5$**−**AM$_7$**. The center of this pseudo-*A*-term correlates well with the UV−vis transitions

https://doi.org/10.1021/acsphyschemau.2c00023
ACS Phys. Chem Au 2022, 2, 468−481

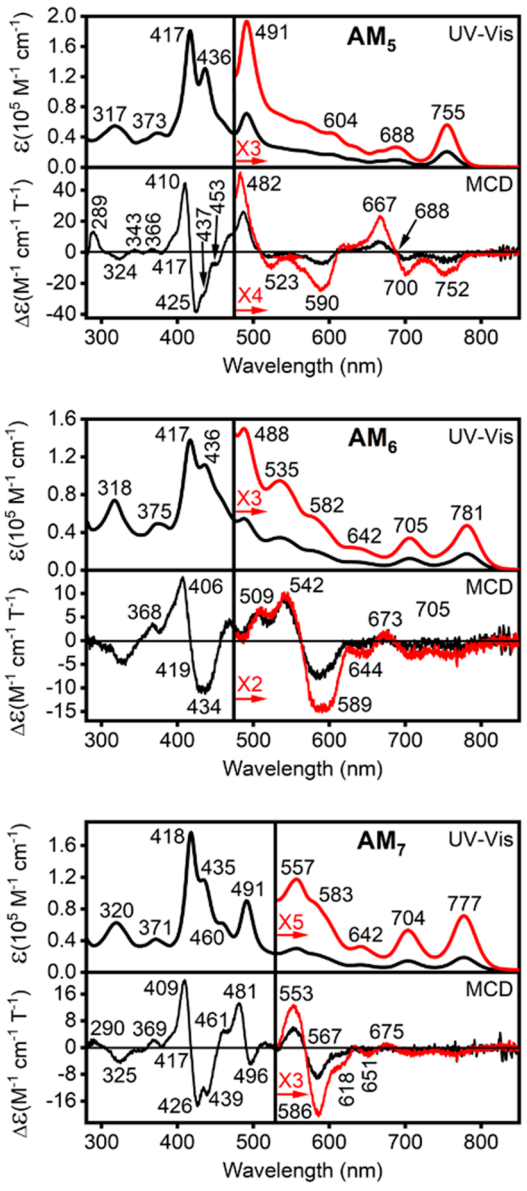

Figure 7. UV−vis and MCD spectra of porphyrins $\mathbf{AM_5}$−$\mathbf{AM_7}$ in DCM.

observed at 688 ($\mathbf{AM_5}$), 705 ($\mathbf{AM_6}$), and 704 ($\mathbf{AM_7}$) nm. Another significantly stronger pseudo-*A*-term was observed in the MCD spectra of porphyrins $\mathbf{AM_5}$−$\mathbf{AM_7}$ between 500 and 560 nm. In general, the intensity of the MCD signals in porphyrins $\mathbf{AM_5}$−$\mathbf{AM_7}$ in the 600−800 spectral envelope is significantly lower compared to the intensity of the MCD bands observed for the porphyrins $\mathbf{AM_1}$−$\mathbf{AM_3}$ in the Q-band region. Such a dramatic decrease in the intensity was also observed in the (doubly-fused by pentacene) bisporphyrins reported earlier.[42] Interestingly, the lowest energy band position in the porphyrins $\mathbf{AM_5}$−$\mathbf{AM_7}$ is nearly constant ($\Delta E \sim 400$ cm^{-1}) and correlates well with an absorption band at 730 nm observed in the UV−vis spectrum of the metal-free bisporphyrin fused by the pentacene bridge. That being said, the red-shifted low-energy bands in shorter π-systems of $\mathbf{AM_5}$−$\mathbf{AM_7}$ (compared to the bisporphyrin analogue) is unexpected. The most resolved MCD spectrum in the Soret band region was observed for $\mathbf{AM_7}$ (Figure 7). In this case, the four most prominent bands observed in the UV−vis spectrum at 491, 460, 435, and 418 nm correlate with two MCD pseudo-*A*-terms centered at 489 and 417 nm and two *B*-terms observed at 461 and 439 nm. Again, the MCD spectra in the Q-band region of porphyrins $\mathbf{AM_5}$−$\mathbf{AM_7}$ have a negative-to-positive amplitude sequence (in ascending energy), which is indicative of the ΔHOMO > ΔLUMO relationship in these compounds.[51−55]

Electrochemistry and Spectroelectrochemistry

Taking into consideration the potential redox activity of the pentacene or pentacenequinone fragments, it was interesting to investigate the redox properties of $\mathbf{AM_1}$−$\mathbf{AM_3}$ and $\mathbf{AM_5}$−$\mathbf{AM_7}$ systems. The summary of the electrochemical data is shown in Table 1, with the representative examples outlined in Figure 8.

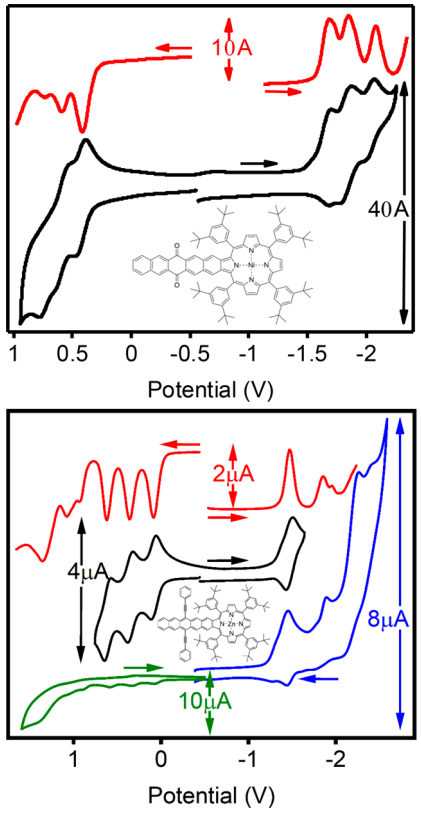

Figure 8. Representative examples of CV and DPV data for $\mathbf{AM_2}$ (top) and $\mathbf{AM_7}$ (bottom) in DCM/0.1 M TBAP system. All potentials are referenced to the Fc/Fc$^+$ couple.

For each compound, multiple oxidation and reduction processes were observed. In the case of the pentacenequinone compounds, three reversible oxidation processes were observed for $\mathbf{AM_1}$ and $\mathbf{AM_2}$ while two reversible and two irreversible processes were observed for $\mathbf{AM_3}$. The first oxidation potential for $\mathbf{AM_1}$−$\mathbf{AM_3}$ spans with a 320 mV range. Three to four reduction processes were observed in $\mathbf{AM_1}$−$\mathbf{AM_3}$ systems. Up to six oxidation processes were observed for the porphyrins $\mathbf{AM_5}$−$\mathbf{AM_7}$, with the first three being reversible. The first oxidation potential in $\mathbf{AM_5}$−$\mathbf{AM_7}$ has a significantly smaller central ion dependency than $\mathbf{AM_1}$−$\mathbf{AM_3}$. Since our DFT calculations discussed below are indicative that the HOMO in $\mathbf{AM_5}$−$\mathbf{AM_7}$ is ∼80% localized on the pentacene fragment, such a small dependency on the central metal ion is not surprising. Multiple reduction processes were also

https://doi.org/10.1021/acsphyschemau.2c00023
ACS Phys. Chem Au 2022, 2, 468−481

observed in $\mathbf{AM_5}$−$\mathbf{AM_7}$, with the first reduction potential being nearly constant.

The formation of a relatively stable charge-separated state upon the photoinduced electron transfer process is key for the performance of porphyrins $\mathbf{AM_1}$−$\mathbf{AM_3}$ and $\mathbf{AM_5}$−$\mathbf{AM_7}$ in light-harvesting modules of organic solar cells. Since these porphyrins are thought to be used as electron donors, the formation and stability of their respective cation-radical forms generated upon a single-electron oxidation condition with controlled potential realized under the spectroelectrochemical conditions were investigated in detail. The single-electron oxidation of the transition-metal centered $\mathbf{AM_2}$ and $\mathbf{AM_3}$ results in the reduction of intensities of the Soret- and Q-band regions and the appearance of new bands at 664 and 901 nm ($\mathbf{AM_2}$) or 699, 753, 854, and 961 nm ($\mathbf{AM_3}$, Figure 9). The cation-radical species formed under spectroelectrochemical conditions are stable and can be almost quantitatively reduced back to the neutral compounds under spectroelectrochemical conditions (Figure S3 in the SI). The oxidation of the metal-free porphyrin $\mathbf{AM_1}$ under spectroelectrochemical conditions also results in the appearance of new NIR bands at 813 and 916 nm (Figure 9). However, reduction of the formed radical-cation species back to the neutral porphyrin is not quantitative and regenerates only ∼70% of the starting material (Figure S3 in the SI). The overall spectroscopic signatures of the cation-radical species $[\mathbf{AM_1}$−$\mathbf{AM_3}]^{+\cdot}$ are typical for the cation-radicals of the traditional tetraarylporphyrins.[56−59] In agreement with the DFT calculations, this indicates a lack of interaction between the outer anthraquinone fragment and the naphthalene-β,β-fused porphyrin. Thus, the quinone carbonyl fragment interrupts the π-conjugation, and the overall spectroscopy of $\mathbf{AM_1}$−$\mathbf{AM_3}$ can be viewed as similar to the naphthalene-β,β-fused porphyrin.

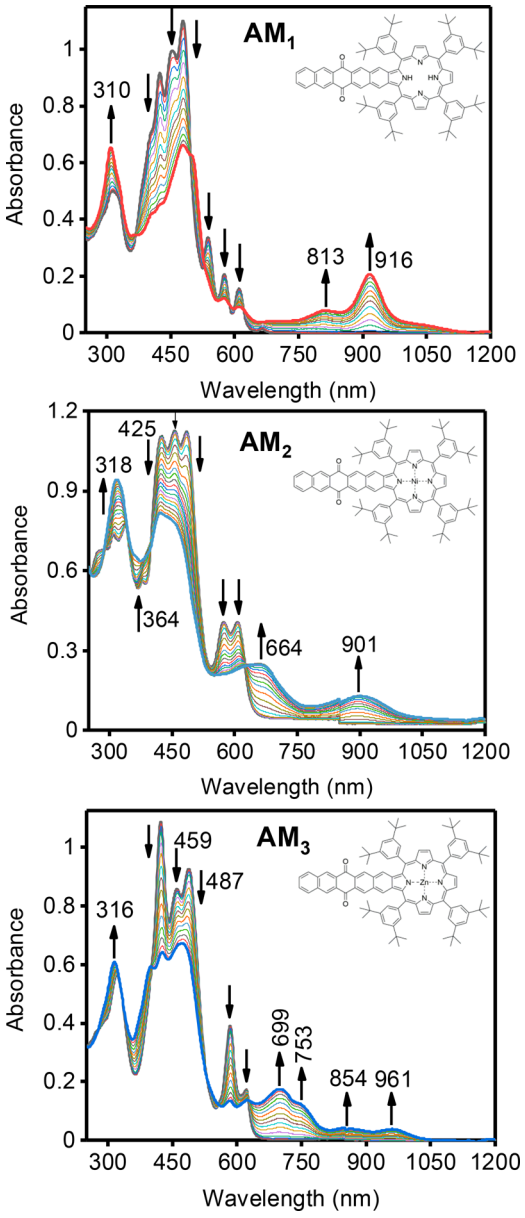

Figure 9. Oxidation of neutral $\mathbf{AM_1}$−$\mathbf{AM_3}$ to $[\mathbf{AM_1}$−$\mathbf{AM_3}]^{+\cdot}$ cation-radicals under spectroelectrochemical conditions in DCM/0.3 M TBAP system.

On the contrary, the single-electron oxidation of the pentacene-fused porphyrins $\mathbf{AM_5}$−$\mathbf{AM_7}$ reveals the different spectroscopic signatures (Figure 10). In particular, a rise of two very intense (∼20 000−50 000 M^{-1} L^{-1}) transitions between 1500 and 2500 nm was observed in each case. The relative intensities of these NIR bands have a clear central-metal dependency with approximately equal intensities observed for $\mathbf{AM_5}$, a significantly stronger lower energy transition for $\mathbf{AM_6}$, and the opposite trend for $\mathbf{AM_7}$. Based on our DFT calculations, the HOMO in $\mathbf{AM_5}$−$\mathbf{AM_7}$ is delocalized over both the porphyrin (∼20%) and pentacene (∼80%) cores, suggesting a significant degree of conjugation between the two chromophores. Thus, it is not surprising to see lower energy transitions in $[\mathbf{AM_5}$−$\mathbf{AM_7}]^{+}$ cation-radicals that have a larger degree of conjugation compared to $[\mathbf{AM_1}$−$\mathbf{AM_3}]^{+}$. However, the large intensity of these bands needs to be carefully explored using modern computational approaches and is a subject of a currently detailed investigation in our laboratories. Again, both transition-metal complexes can be quantitatively reduced from $[\mathbf{AM_6}$−$\mathbf{AM_7}]^{+\cdot}$ cation-radicals to the neutral $\mathbf{AM_6}$−$\mathbf{AM_7}$ (Figure S4 in the SI). However, similar to the case of $[\mathbf{AM_1}]^{+}$, reduction of $[\mathbf{AM_5}]^{+\cdot}$ under spectroelectrochemical conditions does not lead to the quantitative recovery of the neutral $\mathbf{AM_5}$. Indeed, in addition to the expected peaks at 755, 491, and 417 nm, we have observed a significant increase of the 431 nm peak that, unlike in the case of the pure neutral $\mathbf{AM_5}$, has a higher intensity than the 417 nm band.

DFT and TDDFT Calculations

As mentioned above, the UV−vis and MCD spectra of $\mathbf{AM_1}$−$\mathbf{AM_3}$ and $\mathbf{AM_5}$−$\mathbf{AM_7}$ porphyrins and previously reported dinuclear porphyrins bridged by pentacene and pentacenequinone are rather unusual. The complexity of the experimental spectra can be reflective of the presence of two NH tautomers in solution (metal-free compounds only),[60−64] simultaneous conformational isomerism,[65−71] or the nontraditional electronic structure of these compounds. In order to explain the optical and magnetooptical properties of $\mathbf{AM_1}$−$\mathbf{AM_3}$ and $\mathbf{AM_5}$−$\mathbf{AM_7}$ porphyrins, we have conducted an extensive set of DFT and TDDFT calculations on the compounds of interest. First, we optimized the geometries and calculated the energies of conformational isomers as well as NH tautomers using the B3LYP exchange-correlation functional coupled with either the 6-31G(d,p) or 6-311G(d) basis set. In addition, DFT and TDDFT calculations with the M06 exchange-correlation functional were conducted for "twisted" and "bent" con-

https://doi.org/10.1021/acsphyschemau.2c00023
ACS Phys. Chem Au 2022, 2, 468−481

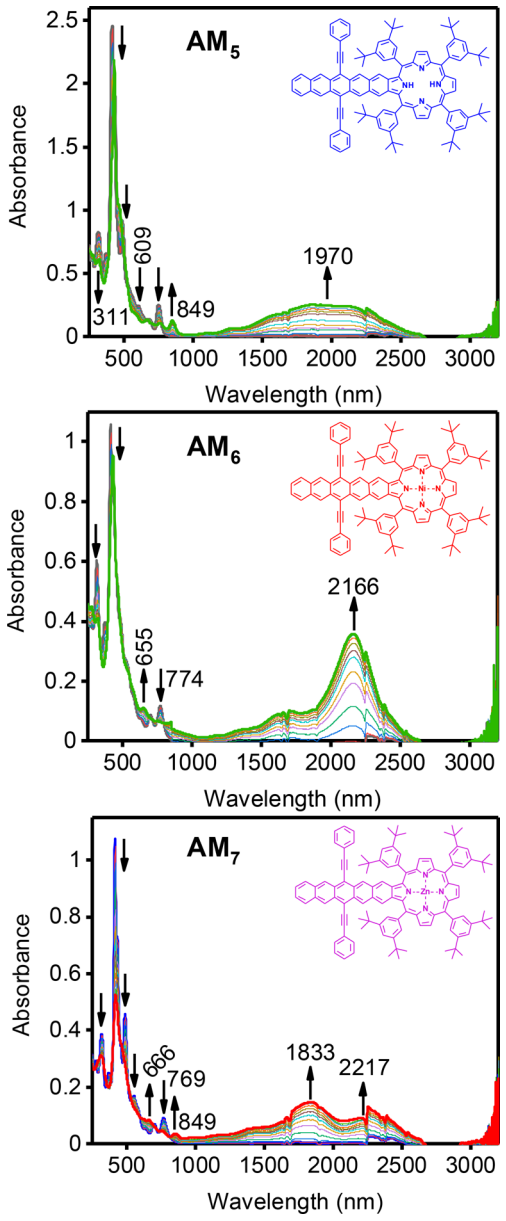

Figure 10. Oxidation of neutral $\mathbf{AM_5}$–$\mathbf{AM_7}$ to $[\mathbf{AM_5}$–$\mathbf{AM_7}]^{+\cdot}$ cation-radicals under spectroelectrochemical conditions in DCM/0.3 M TBAP system.

formations of $\mathbf{AM_2}$ and $\mathbf{AM_6}$ to explore our computational protocol's validity and general trends. It was found that the energies and nature of the frontier orbitals are close for the two basis sets used. DFT calculations with both basis sets also indicate that the only one (the NH tautomer with two NH protons located on the short N–N axis) out of two possible NH tautomers in $\mathbf{AM_1}$ and $\mathbf{AM_5}$ is energetically favorable, and thus, only this tautomer was considered. This is typical for metal-free extended porphyrins, phthalocyanines, and analogues.[72] Next, we found that both "twisted" (twisted porphyrin's π-system and planar pentacene/pentacenequinone fragment) and "bent" (both porphyrin and pentacene/pentacenequinone fragments are planar but have a small angle between them) conformations (Figure 11) are very close in energy and are stable, while the expected classic fully planar conformation in $\mathbf{AM_1}$–$\mathbf{AM_3}$ and $\mathbf{AM_5}$–$\mathbf{AM_7}$ is the transition state (at least one small negative frequency was predicted by

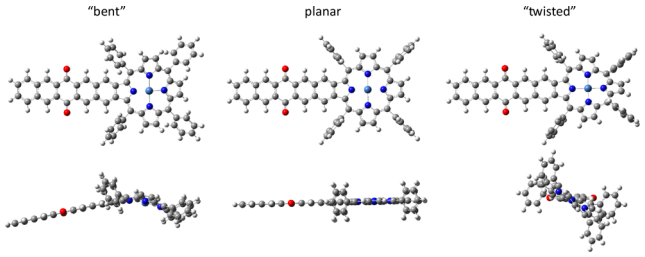

Figure 11. DFT-optimized conformations of $\mathbf{AM_6}$.

DFT). The HOMO in $\mathbf{AM_1}$–$\mathbf{AM_3}$ resembles the classic Gouterman's a_{1u} (in a standard D_{4h} symmetry notation) orbital that is coupled with the appended naphthalene fragment of pentacenequinone (Figure 12). The porphyrin ring contribution to the HOMO is ~80%. This is not typical for the tetra(*meso*-aryl)porphyrins for which a Gouterman's a_{2u}-type HOMO is expected.[73−75] However, taking into consideration the nearly degenerate energies of the a_{1u} and a_{2u} MOs in tetra(*meso*-aryl)porphyrins and the conjugation of the additional π-system of the pentaquinone at the β, β-position of the porphyrin ring, it is not surprising to see the a_{1u}-type MO being the HOMO in $\mathbf{AM_1}$–$\mathbf{AM_3}$. The HOMO−1 in $\mathbf{AM_1}$–$\mathbf{AM_3}$ is localized entirely on the porphyrin π-system and resembles Gouterman's a_{2u} orbital. Taking into consideration the dominant contribution of the porphyrin π-system into the HOMO and HOMO−1 in $\mathbf{AM_1}$–$\mathbf{AM_3}$, it is safe to use the DFT-predicted energies of these two orbitals to define ΔHOMO, which is needed for MCD spectral analysis in these compounds.[51−55] The LUMO region for porphyrins $\mathbf{AM_1}$–$\mathbf{AM_3}$ is somewhat complicated by the interactions between the porphyrin and pentacenequinone π-systems. Indeed, two pairs of orbitals (LUMO/LUMO+3 and LUMO+1/LUMO+2) emerge as the combination of the pentacenequinone MOs and porphyrin-centered Gouterman's $e_g(x)$/$e_g(y)$ pair. The first combination leads to the predominantly (~60%) pentacenequinone-centered LUMO and predominantly (~65%) porphyrin-centered LUMO+3. The second combination results in the predominantly (~75%) porphyrin-centered LUMO+1 and predominantly (~60%) pentacenequinone-centered LUMO+2. If the simplistic way of calculating ΔLUMO is considered (i.e., the energy difference between the LUMO and LUMO+1), then ΔHOMO > ΔLUMO and the negative-to-positive MCD band sequence (in ascending energy) is expected in the MCD spectra of $\mathbf{AM_1}$–$\mathbf{AM_3}$, which, at first glance, agrees with experiment. If the ΔLUMO is calculated using the energy difference between the LUMO+1 and LUMO+2 as two MOs that are dominated by the porphyrin contribution, then ΔHOMO < ΔLUMO and

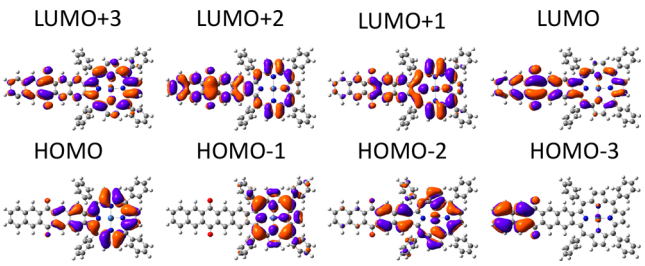

Figure 12. DFT-predicted frontier MOs for "bent" conformations of $\mathbf{AM_2}$ (M06 exchange-correlation functional).

https://doi.org/10.1021/acsphyschemau.2c00023
ACS Phys. Chem Au 2022, 2, 468−481

the positive-to-negative MCD band sequence (in ascending energy) is expected in the MCD spectra of $\mathbf{AM_1}$−$\mathbf{AM_3}$, which, at first glance, disagrees with experiment. As will be discussed below, our TDDFT calculations reveal a significant deviation from such a simplistic description. The DFT-predicted occupied, predominantly pentacenequinone-centered MOs are significantly more stable compared to the frontier porphyrin-centered MOs, which, as expected, are reflective of the electron-deficient nature of the pentacenequinone. The difference between the energies of frontier MOs for the "twisted" and "bent" conformations of $\mathbf{AM_1}$−$\mathbf{AM_3}$ is negligibly small (Figure 13).

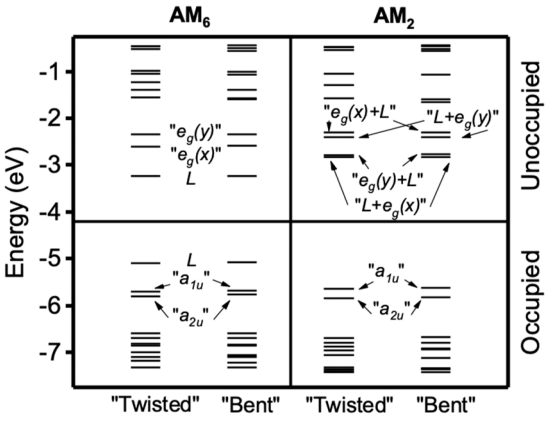

Figure 13. DFT-predicted energy level diagram using the M06 exchange correlation functional. Label "L" represents either pentaquinone or pentacene fragment.

The DFT-predicted HOMO in the pentacene-fused porphyrins $\mathbf{AM_5}$−$\mathbf{AM_7}$ is ∼80% pentacene-centered with only ∼20% contribution from the porphyrin's a_{1u}-type orbital, which is reflective of the strong electron-donating properties of the pentacene fragment (Figure 14). The presence of the

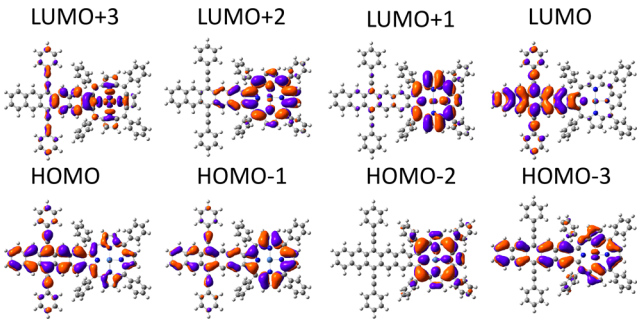

Figure 14. DFT-predicted frontier MOs for "bent" conformations of $\mathbf{AM_6}$ (M06 exchange-correlation functional).

pentacene-centered MO in the HOMO region is also responsible for the richer redox properties observed for the porphyrins $\mathbf{AM_5}$−$\mathbf{AM_7}$ compared to the porphyrins $\mathbf{AM_1}$−$\mathbf{AM_3}$. The HOMO−1 in all complexes is predominantly porphyrin-centered and has a_{1u} character. The HOMO−2 is the localized a_{2u}-type porphyrin-centered orbital in all cases. The DFT-predicted nature of the LUMO in $\mathbf{AM_5}$−$\mathbf{AM_7}$ is also ∼90% localized at the pentacene fragment, while the LUMO+1 and LUMO+2 orbitals are ∼90% localized at the porphyrin ring and resemble Gouterman's e_g pair or the orbitals. The DFT-predicted energies of the a_{1u}/a_{2u} pair in $\mathbf{AM_5}$−$\mathbf{AM_7}$ are close to those predicted in $\mathbf{AM_1}$−$\mathbf{AM_3}$ (Figure 13). Again, if the simple approach for calculating the ΔHOMO/ ΔLUMO ratio is used (HOMO−1/HOMO−2 for ΔHOMO and LUMO+1/LUMO+2 for ΔLUMO), DFT calculations predict the ΔHOMO < ΔLUMO ratio that seemingly contradicts the experimental MCD data.

To gain deeper insight into the properties of the optical and magnetooptical transitions observed in the porphyrins $\mathbf{AM_1}$−$\mathbf{AM_3}$ and $\mathbf{AM_5}$−$\mathbf{AM_7}$, we have conducted TDDFT calculations on the nickel complexes $\mathbf{AM_2}$ and $\mathbf{AM_6}$ using the B3LYP and M06 exchange-correlation functionals on both "twisted" and "bent" conformations (Figure 15 and Figure S5 in the SI). In

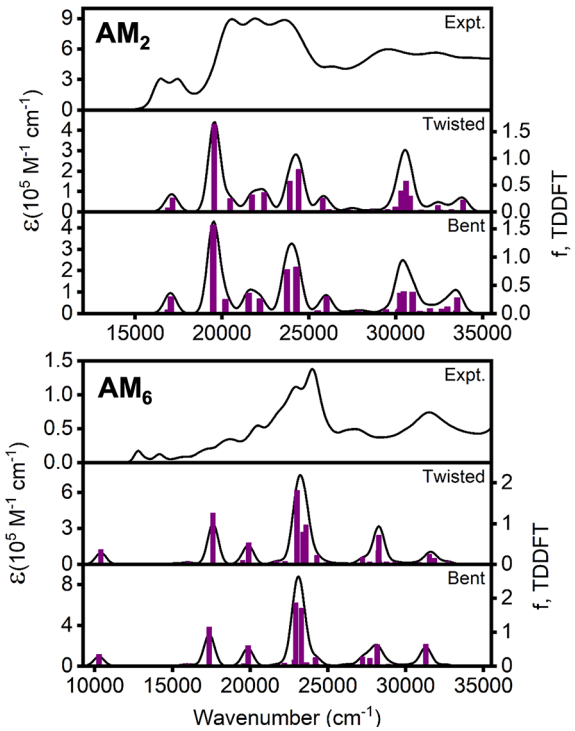

Figure 15. TDDFT-predicted UV−vis spectra of $\mathbf{AM_2}$ and $\mathbf{AM_6}$ using the M06 exchange correlation functional.

general, TDDFT predicted spectra for the porphyrin $\mathbf{AM_2}$ correlate well with the experimental data. First, from the TDDFT calculations, it is clear that the conformational change between "twisted" and "bent" structures does not significantly alter the energies, intensities, and nature of the TDDFT-predicted spectra. This is not surprising as the energies of these two conformations are very close to each other. Next, results for the TDDFT calculations with the B3LYP and M06 exchange-correlation functionals are close to each other with a small high-energy shift for the predicted vertical excitation energies observed in the case of the M06 calculations, which is expected[76,77] as the latter functional has a higher percentage of Hartree−Fock exchange. Thus, in order to simplify further discussion, only the M06 TDDFT results will be discussed below. The first two excitations predicted by TDDFT with significant intensity for $\mathbf{AM_2}$ (excited states 5 and 6) are dominated by the HOMO (∼80% porphyrin-centered a_{1u}-type MO) → LUMO+1 (∼75% porphyrin-centered $e_g(x)$-type MO) and HOMO (∼80% porphyrin-centered a_{1u}-type MO) → LUMO (∼40% porphyrin-centered $e_g(y)$-type MO) single-electron excitations, respectively. Since ∼60% of the electron

https://doi.org/10.1021/acsphyschemau.2c00023
ACS Phys. Chem Au 2022, 2, 468−481

Table 2. TDDFT-Predicted Properties for Selected Excited States for AM_2 and AM_6 Using the M06 Exchange Correlation Functional and Twisted Geometry

excited state	energy, cm^{-1}	wavelength, nm	oscillator strength, f	contributions
			AM_2	
5	16 886	592	0.0741	H→L+1 (66%), H-1→L (12%), H-24→L+5 (8%), H-1→L+3 (6%), H→L+2 (2%)
6	17 165	583	0.2589	H→L (60%), H-1→L+1 (27%), H→L+3 (10%), H-1→L+2 (2%)
7	19 564	511	1.6350	H-1→L+1 (52%), H→L (36%), H→L+3 (6%)
8	20 478	488	0.2417	H-1→L (46%), H→L+2 (28%), H→L+1 (20%), H-1→L+3 (3%)
9	21 734	460	0.3151	H→L+2 (55%), H-1→L (38%), H-1→L+3 (4%)
10	22 432	446	0.3597	H→L+3 (50%), H-1→L+2 (26%), H-1→L+1 (19%)
12	23 916	418	0.5698	H-1→L+2 (60%), H→L+3 (32%), H-2→L (3%)
13	24 426	409	0.7892	H-1→L+3 (80%), H→L+2 (10%), H→L+1 (3%)
16	25 814	387	0.2549	H-3→L (55%), H-4→L+1 (18%), H-2→L (6%), H-3→L+3 (5%), H-5→L (4%), H→L+5 (2%), H-4→L+2 (2%)
			AM_6	
1	10 405	961	0.3551	H→L (100%)
5	15 179	659	0.0265	H-1→L (54%), H→L+1 (37%), H-2→L+2 (4%), H-1→L+1 (4%)
6	15 999	625	0.0609	H→L+1 (52%), H-1→L (42%), H-1→L+1 (3%), H-2→L+2 (3%)
9	17 612	568	1.2570	H→L+2 (61%), H-2→L (32%), H-1→L+2 (3%), H-2→L+1 (3%)
10	19 527	512	0.0983	H-1→L+1 (64%), H-2→L+2 (21%), H→L+1 (8%), H-3→L (3%)
11	19 913	502	0.5291	H-2→L+1 (59%), H-1→L+2 (19%), H→L+2 (14%), H-2→L (3%)
12	21 697	461	0.0817	H-3→L (50%), H-4→L (43%)
13	22 243	450	0.0660	H-4→L (46%), H-3→L (28%), H→L+3 (9%), H-3→L+1 (7%), H-6→L+1 (5%)
14	22 942	436	0.0303	H→L+3 (68%), H-6→L (9%), H-3→L+1 (6%), H-1→L+1 (4%), H-6→L+1 (4%), H-3→L (2%)
15	23 014	435	1.8150	H-1→L+2 (44%), H-2→L+1 (19%), H-5→L (19%), H-9→L (14%)
16	23 397	427	0.7892	H-6→L (36%), H→L+3 (19%), H-3→L+1 (14%), H-2→L+2 (12%), H-6→L+1 (5%), H-3→L (4%), H-4→L+1 (3%), H-4→L (3%), H-1→L+1 (2%)
17	23 589	424	0.9630	H-2→L+2 (57%), H-1→L+1 (21%), H-6→L (12%), H-3→L+1 (4%), H-6→L+1 (3%)
20	24 302	411	0.2199	H→L+4 (94%), H-1→L+4 (4%)
21	24 896	402	0.0385	H→L+5 (65%), H-1→L+5 (31%)

density in LUMO is pentacenequinone-centered, the latter can be considered as substantially charge-transfer (porphyrin-to-pentacenequinone) in character (Table 2). Both excited states, however, resemble, to some extent, Gouterman's Q-band transitions.[49,50] More importantly, these excited states were predicted to be only ~280 cm^{-1} apart (592 and 583 nm), and thus, this explains extremely well the observation of the MCD pseudo-*A*-term observed at 609 nm. TDDFT calculations predict that three prominent bands in the Soret region (experimentally observed between 490 and 420 nm) can originate from six excited states. The experimentally observed band at 486 nm in **AM_2** correlates well with the very strong TDDFT-predicted one at 511 nm (excited state 7), which is dominated by the HOMO−1 (~100% porphyrin-centered a_{2u}-type MO) → LUMO+1 single-electron excitation. The experimental absorption at 456 nm correlates well with the energies of TDDFT-predicted excited states 9 and 10 (460 and 446 nm, respectively). These are dominated by the HOMO → LUMO+2 and HOMO → LUMO+3 single-electron excitations, respectively. Finally, the experimentally observed band at 424 nm correlates well with the TDDFT-predicted (418 and 409 nm) excited states 12 and 13, which are dominated by HOMO−1 → LUMO+2 and HOMO−1 → LUMO+3 single-electron excitations. The overall shape of the experimental UV−vis and MCD spectra in **AM_2** is reflective of the "2 + 4" orbital active space that consists of two close-energy spaced HOMO−HOMO−1 and four close-energy spaced LUMO−LUMO+3 orbitals, which form eight excited states that are dominated by single-electron excitations from/to these orbitals (Table 2). HOMO and HOMO−1 resemble the classic Gouterman's a_{1u} and a_{2u} MOs, while LUMO−LUMO+3 MOs are reflective of the linear combination of the Gouterman's e_g set and two MOs of the pentacenequinone. Thus, the classic Gouterman's four-orbital model[49,50] is not applicable for the description of the UV−vis and MCD spectroscopy of the **AM_2** porphyrin. However, the TDDFT calculations provide a very reasonable explanation of its spectroscopy.

The situation becomes more complex in the case of reduced, pentacene-fused porphyrin **AM_6** (Figure 15). In this case, for the description of the UV−vis and MCD spectra, one needs to consider "3 + 3" (HOMO−HOMO−2 and LUMO−LUMO+2) orbital active space. Moreover, since the HOMO and LUMO are heavily localized on the pentacene fragment, one would expect the presence of the low-energy $\pi-\pi^*$ transition localized on the pentacene. Indeed, TDDFT predicts that the first excited state in **AM_6** should have a significant intensity and originates exclusively from the HOMO → LUMO single-electron excitation (Table 2). In agreement with this prediction, the MCD signal associated with the relatively strong ~780 nm band in the UV−vis spectra of **AM_6**−**AM_7** porphyrins is very weak (Figure 7). The next two relatively weak transitions were predicted at 659 and 625 nm by TDDFT calculations and are dominated by the HOMO−1 → LUMO and HOMO → LUMO+1 single-electron excitations, making them heavily charge-transfer in nature. These two transitions can be responsible for a weak MCD pseudo-*A*-term observed at ~680 nm in the spectra of **AM_6** and **AM_7**. A very strong band predicted by the TDDFT calculations at 568 nm is dominated by HOMO → LUMO+2 and HOMO−2 → LUMO single-electron excitations (Table 2). This excited state, again, has a predominant charge-transfer character and correlates well with the MCD *B*-term observed between 618

https://doi.org/10.1021/acsphyschemau.2c00023
ACS Phys. Chem Au 2022, 2, 468−481

and 585 nm in the spectra of **AM$_6$** and **AM$_7$**. The next pair of relatively intense transitions was predicted at 512 and 502 nm. These are dominated by HOMO−1 → LUMO+1 and HOMO−2 → LUMO+1 single-electron excitations, respectively. These are centered at the porphyrin core and might be responsible for the MCD pseudo-*A*-term centered at ∼560 nm in the spectra of **AM$_6$** and **AM$_7$**. Finally, TDDFT calculations predict that the 400−450 nm spectral envelope in the UV−vis and MCD spectra of **AM$_6$** should be dominated by three excited states (excited states 15−17, Table 2). The excited states 15 and 17 have clear porphyrin-centered $\pi-\pi^*$ excitation nature, while the excited state 16 has a significant charge-transfer character. More importantly, excited states 10 and 15 and 11 and 17 form two pairs ($a_{1u} \rightarrow e_g(x)/e_g(y)$ for the excited states 10 and 15 and $a_{2u} \rightarrow e_g(x)/e_g(y)$ for the excited states 11 and 17), which is characteristic for bacteriochlorines, thus highlighting a strong perturbation of the porphyrin's π-system by conjugation with the pentacene fragment. Overall, the classic Gouterman's four-orbital model is not applicable in the description of the UV−vis and MCD spectra of pentacenequinone- or pentacene-fused porphyrins. To a large extent, the spectroscopy of the pentacenequinone-fused porphyrins can be explained using the "2 + 4" active space, while the spectroscopy of the pentacene-fused porphyrins can be explained using the "3 + 3" active space.

Stability Studies

The stability of **AM$_5$**−**AM$_7$** was examined through photodegradation in an oxygenated benzene solution with a 0.01 mM pentacene concentration under ambient light irradiation (Figures S6−S8 in the SI). The decomposition half-life was determined through monitoring of the disappearance of the most red-shifted absorption band over time. The half-life of Ni(II) pentacene-fused porphyrin **AM$_6$** was estimated to be >28.3 days. In sharp contrast, its free base and Zn(II) analogues **AM$_5$** and **AM$_7$** displayed a much shorter decomposition half-life. The half-life of **AM$_5$** was measured as 1.3 days (31.2 h), and the half-life of **AM$_7$** was found to be 1.2 days (28.8 h). Despite their decreased stability compared with that of **AM$_6$**, the stability of **AM$_5$** and **AM$_7$** are similar to the most stable pentacene **BPE-P** (33 h, Figure 1). Given that one electron-rich pyrrole is fused to the pentacene in these pentacene-fused porphyrins, **AM$_5$**−**AM$_7$** are more like pseudohexacenes. **AM$_5$**−**AM$_7$** are still much more stable than the corresponding hexacene. These data suggest that the center metal of porphyrin plays a critical role in determining the stability of these fused systems, confirming our earlier study that Ni(II) porphyrin creates a short-lived intermediate charge-transfer state blocking the photodegradation pathways and thus significantly stabilizing the fused pentacenes.

CONCLUSIONS

Largely π-extended systems represent an exciting research in frontier science. Conjugated systems incorporating two or more chromophores are challenging to achieve. Through utilizing a Pd(0)-catalyzed cascade reaction of acrolein and dibromoporphyrins, unsymmetric pentacenequinone- and pentacene-fused porphyrins have been obtained. Although they have similar symmetry, the cross-conjugated (**AM$_1$**−**AM$_3$**) and linear-conjugated molecular systems displayed strikingly different electronic and optical properties, both of which are unusually complex and nontypical of porphyrins. While **AM$_1$**−**AM$_3$** showed abnormal splitting patterns and large absorption ranges spanning from 250 to 550 nm for the "Soret" band, **AM$_5$**−**AM$_7$** displayed narrow and doubly split Soret bands with a large number of unexpected absorptions in the Q-band region (500−800 nm). CV revealed rich redox profiles for both the cross-conjugated and linear-conjugated π-extended porphyrins with up to six oxidation processes observed for **AM$_5$**−**AM$_7$**. Both **AM$_1$**−**AM$_3$** and **AM$_5$**−**AM$_7$** formed stable radical cations under spectroelectrochemical conditions, suggesting the exceptional ability of these cross- and linear-conjugated π-extended systems to accommodate charges. [**AM$_5$**−**AM$_7$**]$^+$ cation-radicals exhibited exceptionally strong absorption bands in the IR region between 1500 and 2500 nm. While the low energy transition can be attributed to the large π-extension, the huge intensity of these bands remains elusive and is worthy of further investigation. MCD and TDDFT calculations suggest that the existence of multiple charge transfer states contributes to the complex spectra of **AM$_1$**−**AM$_7$**. The classical Gouterman's four-orbital model created for porphyrin systems was not suitable to interpret and understand the complex spectra of **AM$_1$**−**AM$_7$**. The UV−vis and MCD spectra of pentaquinone- and pentacene-fused porphyrins were successfully resolved through "2 + 4" and "3 + 3" active spaces, respectively.

Ni(II) pentacene-fused porphyrin (**AM$_6$**) displayed unusually high stability similar to the Ni(II) pentacene-fused porphyrin dimer,[30] and is significantly more stable than the relevant pentacene and hexacene derivatives. In contrast, when the center metal of the porphyrin was replaced with free-base and Zn(II), the stability of **AM$_5$** and **AM$_7$** dropped to levels similar to those of pentacene derivatives. This work proves that incorporation of Ni(II) porphyrin is an effective strategy to stabilize longer acenes. Ni(II) porphyrin-fused heptacene and nonacene are currently being prepared in our laboratory. The effects of the center metal of porphyrins and the substituent highlight the high tunability of these materials. This work has demonstrated that fusion of acenes and other polycyclic aromatic hydrocarbons (PAHs) at porphyrin β, β-positions could become a powerful tool to construct novel classes of largely π-extended organic materials, providing new opportunities in basic science and applications.

ASSOCIATED CONTENT

Supporting Information

The Supporting Information is available free of charge at https://pubs.acs.org/doi/10.1021/acsphyschemau.2c00023.

Experimental procedures, ^{1}H and ^{13}C NMR and other characterization data, single crystal X-ray analysis, computational methods (PDF)

Crystallographic data for the **AM$_1$** complex (CIF)

Crystallographic data for **AM$_2$** (CIF)

AUTHOR INFORMATION

Corresponding Authors

Hong Wang − *Department of Chemistry, University of North Texas, Denton, Texas 76203-5017, United States;* orcid.org/0000-0001-7947-2083; Email: hong.wang@unt.edu

Victor N. Nemykin − *Department of Chemistry, University of Manitoba, Winnipeg, MB R3T 2N2, Canada; Department of Chemistry, University of Tennessee, Knoxville, Tennessee 37996-1600, United States;* orcid.org/0000-0003-4345-0848; Email: vnemykin@utk.edu

https://doi.org/10.1021/acsphyschemau.2c00023
ACS Phys. Chem Au 2022, 2, 468−481

Authors

Austen Moss − *Department of Chemistry, University of North Texas, Denton, Texas 76203-5017, United States*

Dustin E. Nevonen − *Department of Chemistry, University of Manitoba, Winnipeg, MB R3T 2N2, Canada*

Yi Hu − *Department of Chemistry, University of North Texas, Denton, Texas 76203-5017, United States*

Vladimir N. Nesterov − *Department of Chemistry, University of North Texas, Denton, Texas 76203-5017, United States*

Complete contact information is available at: https://pubs.acs.org/10.1021/acsphyschemau.2c00023

Author Contributions

†A.M. and D.E.N. authors contributed equally. The manuscript was written through contributions of all authors.

Funding

This work was supported by the U.S. Department of Energy, Office of Science, Basic Energy Sciences under Award (DE-SC0016766). We acknowledge the National Science Foundation MRI Program (CHE-1726652) and the University of North Texas for supporting the acquisition of the Rigaku XtaLAB Synergy-S X-ray diffractometer. VNN wish to acknowledge support from the WestGrid Canada and the University of Tennessee.

Notes

The authors declare no competing financial interest.

■ ACKNOWLEDGMENTS

Our gratitude goes out to Dr. Guido Verbeck and the Laboratory for Imaging Mass Spectrometry at the University of North Texas for MALDI-Orbitrap Mass Spectrometry data. VNN acknowledge the University of Tennessee and WestGrid Canada for support.

■ ABBREVIATIONS

DCM, dichloromethane; TBAP, tetrabutylammonium perchlorate; TLC, thin layer chromatography; SI, electronic Supporting Information

■ REFERENCES

(1) Stepien, M.; Gonka, E.; Zyla, M.; Sprutta, N. Heterocyclic Nanographenes and Other Polycyclic Heteroaromatic Compounds: Synthetic Routes, Properties, and Applications. *Chem. Rev.* **2017**, *117* (4), 3479−3716.

(2) Narita, A.; Wang, X. Y.; Feng, X.; Mullen, K. New advances in nanographene chemistry. *Chem. Soc. Rev.* **2015**, *44* (18), 6616−6643.

(3) Ono, N.; Yamada, H.; Okujima, T. Synthesis of Porphyrins Fused with Aromatic Rings. In *Handbook of Porphyrin Science*; Kadish, K. M., Smith, K. M., Guilard, R., Eds.; World Scientific, 2010; Chapter 7.

(4) Carvalho, C. M.; Brocksom, T. J.; de Oliveira, K. T. Tetrabenzoporphyrins: synthetic developments and applications. *Chem. Soc. Rev.* **2013**, *42* (8), 3302−3317.

(5) Cheprakov, A. V.; Filatov, M. A. The Dihydroisoindole Approach to Lineraly Annelated π-Extended Porphyrins. *J. Porphyrins Phthalocyanines* **2009**, *13*, 291−303.

(6) Hayashi, S.; Tanaka, M.; Hayashi, H.; Eu, S.; Umeyama, T.; Matano, Y.; Araki, Y.; Imahori, H. Naphthyl-Fused π-Elongated Porphyrins for Dye-Sensitized TiO_2 Cells. *J. Phys. Chem. C* **2008**, *112*, 15576−15585.

(7) Ball, J. M.; Davis, N. K. S.; Wilkinson, J. D.; Kirkpatrick, J.; Teuscher, J.; Gunning, R.; Anderson, H. L.; Snaith, H. J. A panchromatic anthracene-fused porphyrin sensitizer for dye-sensitized solar cells. *RSC Adv.* **2012**, *2* (17), 6846−6853.

(8) Wang, C.-L.; Chang, Y.-C.; Lan, C.-M.; Lo, C.-F.; Wei-Guang Diau, E.; Lin, C.-Y. Enhanced light harvesting with π-conjugated cyclic aromatic hydrocarbons for porphyrin-sensitized solar cells. *Energy Environ. Sci.* **2011**, *4* (5), 1788.

(9) Roznyatovskiy, V. V.; Lee, C. H.; Sessler, J. L. π-Extended isomeric and expanded porphyrins. *Chem. Soc. Rev.* **2013**, *42* (5), 1921−1933.

(10) Boerner, L. J. K.; Mazumder, S.; Pink, M.; Zaleski, J. M.; Baik, M.-H. Conformational and Electronic Consequences in Crafting Extended, π-Conjugated, Light Harvesting Macrocycles. *Chem.—Eur. J.* **2011**, *17*, 14539−14551.

(11) Kobayashi, N.; et al. Ring-expanded porphyrins as an approach towards highly conductive molecular semiconductors. *Chem. Phys. Lett.* **1993**, *205*, 51−54.

(12) Lash, T. D. Modification of the porphyrin chromophore by ring fusion: identifying trends due to annelation of the porphyrin nucleus. *J. Porphyrins Phthalocyanines* **2001**, *5*, 267−288.

(13) Yamada, H.; Kuzuhara, D.; Takahashi, T.; Shimizu, Y.; Uota, K.; Okujima, T.; Uno, H.; Ono, N. Synthesis and Characterization of Tetraanthroporphyrins. *Org. Lett.* **2008**, *10* (14), 2947−2950.

(14) Davis, N. K. S.; Thompson, A. L.; Anderson, H. L. A Porphyrin Fused to Four Anthracenes. *J. Am. Chem. Soc.* **2011**, *133*, 30−31.

(15) Lewtak, J. P.; Gryko, D. T. Synthesis of π-extended porphyrins via intramolecular oxidative coupling. *Chem. Commun.* **2012**, *48* (81), 10069−10086.

(16) Mysliwiec, D.; Donnio, B.; Chmielewski, P. J.; Heinrich, B.; Stepien, M. Peripherally fused porphyrins via the Scholl reaction: synthesis, self-assembly, and mesomorphism. *J. Am. Chem. Soc.* **2012**, *134* (10), 4822−4833.

(17) Chen, P.; Fang, Y.; Kadish, K. M.; Lewtak, J. P.; Koszelewski, D.; Janiga, A.; Gryko, D. T. Electrochemically driven intramolecular oxidative aromatic coupling as a pathway toward pi-extended porphyrins. *Inorg. Chem.* **2013**, *52* (16), 9532−9538.

(18) Koszelewski, D.; Nowak-Król, A.; Drobizhev, M.; Wilson, C. J.; Haley, J. E.; Cooper, T. M.; Romiszewski, J.; Górecka, E.; Anderson, H. L.; Rebane, A.; et al. Synthesis and linear and nonlinear optical properties of low-melting π-extended porphyrins. *J. Mater. Chem. C* **2013**, *1* (10), 2044−2053.

(19) Fang, Y.; Koszelewski, D.; Kadish, K. M.; Gryko, D. T. Facile electrosynthesis of pi-extended porphyrins. *Chem. Commun.* **2014**, *50* (64), 8864−8867.

(20) Fukui, N.; Yorimitsu, H.; Osuka, A. meso,beta-Oligohaloporphyrins as Useful Synthetic Intermediates of Diphenylamine-Fused Porphyrin and meso-to-meso beta-to-beta Doubly Butadiyne-Bridged Diporphyrin. *Angew. Chem., Int. Ed.* **2015**, *54* (21), 6311−6314.

(21) Fukui, N.; Lee, S. K.; Kato, K.; Shimizu, D.; Tanaka, T.; Lee, S.; Yorimitsu, H.; Kim, D.; Osuka, A. Regioselective phenylene-fusion reactions of Ni(ii)-porphyrins controlled by an electron-withdrawing meso-substituent. *Chem. Sci.* **2016**, *7* (7), 4059−4066.

(22) Fukui, N.; Osuka, A. Singly and Doubly 1,2-Phenylene-Inserted Porphyrin Arch-Tape Dimers: Synthesis and Highly Contorted Structures. *Angew. Chem., Int. Ed.* **2018**, *57* (21), 6304−6308.

(23) Hooper, R. W.; Zhang, A.; Koszelewski, D.; Lewtak, J. P.; Koszarna, B.; Levy, C. J.; Gryko, D. T.; Stillman, M. J. Differential quenching of the angular momentum of the B and Q bands of a porphyrin as a result of extended ring π-conjugation. *J. Porphyrins Phthalocyanines* **2018**, *22* (12), 1111−1128.

(24) Kato, K.; Furukawa, K.; Mori, T.; Osuka, A. Porphyrin-Based Air-Stable Helical Radicals. *Chem.—Eur. J.* **2018**, *24* (3), 572−575.

(25) Chaudhary, A.; Srinivasan, A.; Chandrashekar, T. K. *The Handbook of Porphyrin Science*; Kadish, K. M., Smith, K. M., Guilard, G., Eds.; World Scientific: Singapore, 2014; Vol. *32*, p 271.

(26) Reimers, J. R.; Hall, L. E.; Crossley, M. J.; Hush, N. S. Rigid Fused Oligoporphyrins as Potential Versatile Molecular Wires. 2. B3LYP and SCF Calculated Geometric and Electronic Properties of 98 Oligoporphyrin and Related Molecules. *J. Phys. Chem. A* **1999**, *103*, 4385−4397.

(27) Dover, C. B.; Gallaher, J. K.; Frazer, L.; Tapping, P. C.; Petty, A. J., 2nd; Crossley, M. J.; Anthony, J. E.; Kee, T. W.; Schmidt, T. W. Endothermic singlet fission is hindered by excimer formation. *Nat. Chem.* **2018**, *10* (3), 305−310.
(28) Canfield, P. J.; Blake, I. M.; Cai, Z.-L.; Luck, I. J.; Krausz, E.; Kobayashi, R.; Reimers, J. R.; Crossley, M. J. A new fundamental type of conformational isomerism. *Nat. Chem.* **2018**, *10* (6), 615−624.
(29) Crossley, M. J.; Johnston, L. A. Laterally-extended porphyrin systems incorporating a switchable unit. *Chem. Commun.* **2002**, *10*, 1122−1123.
(30) Birin, K. P.; Poddubnaya, A. I.; Abdulaeva, I. A.; Gorbunova, Y. G.; Tsivadze, A. Y. Revisiting 2,3-diaminoporphyrins: key synthons for heterocycle-appended porphyrins. *Dyes Pigm.* **2018**, *156*, 243−249.
(31) Ou, Z.; Khoury, T.; Fang, Y.; Zhu, W.; Sintic, P. J.; Crossley, M. J.; Kadish, K. M. Gold(III) porphyrins containing two, three, or four beta,beta'-fused quinoxalines. Synthesis, electrochemistry, and effect of structure and acidity on electroreduction mechanism. *Inorg. Chem.* **2013**, *52* (5), 2474−2483.
(32) Reek, J. N. H.; Rowan, A. E.; de Gelder, R.; Beurskens, P. T.; Crossley, M. J.; De Feyter, S.; de Schryver, F.; Nolte, R. J. M. Novel Cleft-Containing Porphyrins as Models for Studying Electron Transfer Processes. *Angew. Chem., Int. Ed.* **1997**, *36*, 361−363.
(33) Crossley, M. J.; Burn, P. L. An Approach to Porphyrin-based Molecular Wires: Synthesis of a Bis(porphyrin)tetraone and its Conversion to a Linearly Conjugated Tetrakisporphyrin System. *J. Chem. Soc., Chem. Commun.* **1991**, 1569−1571.
(34) Finikova, O. S.; Cheprakov, A. V.; Carroll, P. J.; Vinogradov, S. A. Novel Route to Functionalized Tetraaryltetra[2,3]-naphthaloporphyrins via Oxidative Aromatization. *J. Org. Chem.* **2003**, *68*, 7517−7520.
(35) Finikova, O. S.; Aleshchenkov, S. E.; Brinas, R. P.; Cheprakov, A. V.; Carroll, P. J.; Vinogradov, S. A. Synthesis of Symmetrical Tetraaryltetranaphtho[2,3]porphyrins. *J. Org. Chem.* **2005**, *70*, 4617−4628.
(36) Esipova, T. V.; Vinogradov, S. A. Synthesis of phosphorescent asymmetrically pi-extended porphyrins for two-photon applications. *J. Org. Chem.* **2014**, *79* (18), 8812−8825.
(37) Filatov, M. A.; Heinrich, E.; Landfester, K.; Baluschev, S. meso-Tetraphenylporphyrin with a pi-system extended by fusion with anthraquinone. *Org. Biomol. Chem.* **2015**, *13* (25), 6977−6983.
(38) Lewtak, J. P.; Gryko, D. T. Synthesis of π-extended porphyrins via intramolecular oxidative coupling. *Chem. Commun.* **2012**, *48* (81), 10069−10086.
(39) Cheprakov, A. V. The Synthesis of pi-Extended Porphyrins. In *Handbook of Porphyrin Science-With Applications to Chemistry, Physics, Material Science, Engineering, Biology and Medicine*; Smith, K. M., Kadish, K. M., Guilard, R., Eds.; World Scientific: Singapore, 2011.
(40) Deshpande, R.; Jiang, L.; Schmidt, G.; Rakovan, J.; Wang, X.; Wheeler, K.; Wang, H. A concise approach to the synthesis of opp-dibenzoporphyrins through the Heck reaction. *Org. Lett.* **2009**, *11*, 4251−4253.
(41) Jiang, L.; Engle, J. T.; Sirk, L.; Hartley, C. S.; Ziegler, C. J.; Wang, H. Triphenylene-Fused Porphyrins. *Org. Lett.* **2011**, *13*, 3020−3023.
(42) Jiang, L.; Engle, J. T.; Zaenglein, R. A.; Matus, A.; Ziegler, C. J.; Wang, H.; Stillman, M. J. Pentacene-fused diporphyrins. *Chem.—Eur. J.* **2014**, *20* (43), 13865−13870.
(43) Hu, Y.; Thomas, M. B.; Webre, W. A.; Moss, A.; Jinadasa, R. G. W.; Nesterov, V. N.; D'Souza, F.; Wang, H. Nickel(II) Bisporphyrin-Fused Pentacenes Exhibiting Abnormal High Stability. *Angew. Chem., Int. Ed.* **2020**, *59*, 20075−20082.
(44) Jiang, L.; Zaenglein, R. A.; Engle, J. T.; Mittal, C.; Hartley, C. S.; Ziegler, C. J.; Wang, H. Water-soluble ionic benzoporphyrins. *Chem. Commun.* **2012**, *48* (55), 6927−6929.
(45) Jinadasa, R. G.; Fang, Y.; Kumar, S.; Osinski, A. J.; Jiang, X.; Ziegler, C. J.; Kadish, K. M.; Wang, H. β-Functionalized Push-Pull opp-Dibenzoporphyrins. *J. Org. Chem.* **2015**, *80* (24), 12076−12087.
(46) Gholami, M.; Tykwinski, R. R. Oligomeric and Polymeric Systems with a Cross-conjugated π-Framework. *Chem. Rev.* **2006**, *106*, 4997−5027.
(47) Zucchero, A. J.; Mcgrier, P. L.; Bunz, U. H. F. Cross-Conjugated Cruciform Fluorophores. *Acc. Chem. Res.* **2010**, *43* (3), 397−408.
(48) Banala, S.; Rühl, T.; Wurst, K.; Kräutler, B. "Blackening" porphyrins by conjugation with quinones. *Angew. Chem., Int. Ed.* **2009**, *48* (3), 599−603.
(49) Gouterman, M. J. *The Porphyrins*; Academic Press, 1978.
(50) Gouterman, M. J. Spectra of Porphyrins. *Mol. Spectrosc.* **1961**, *6*, 138−163.
(51) Waluk, J.; Muller, M.; Swiderek, P.; Kocher, M.; Vogel, E.; Hohlneicher, G.; Michl, J. Electronic states of porphycenes. *J. Am. Chem. Soc.* **1991**, *113*, 5511−5527.
(52) Waluk, J.; Michl, J. Perimeter model and magnetic circular dichroism of porphyrin analogs. *J. Org. Chem.* **1991**, *56*, 2729−2735.
(53) Michl, J. Magnetic circular dichroism of aromatic molecules. *Tetrahedron* **1984**, *40*, 3845−3934.
(54) Michl, J. Magnetic circular dichroism of cyclic. pi.-electron systems. 2. Algebraic solution of the perimeter model for the B terms of systems with a (4N + 2)-electron [n]annulene perimeter. *J. Am. Chem. Soc.* **1978**, *100*, 6812−6818.
(55) Michl, J. Magnetic circular dichroism of cyclic. pi.-electron systems. 1. Algebraic solution of the perimeter model for the A and B terms of high-symmetry systems with a (4N + 2)-electron [n]annulene perimeter. *J. Am. Chem. Soc.* **1978**, *100*, 6801−6811.
(56) Xue, S.; Ou, Z.; Ye, L.; Lu, G.; Fang, Y.; Jiang, X.; Kadish, K. M. Effect of Solvent and Protonation/Deprotonation on Electrochemistry, Spectroelectrochemistry and Electron-Transfer Mechanisms of N-Confused Tetraarylporphyrins in Nonaqueous Media. *Chem.—Eur. J.* **2015**, *21*, 2651−2661.
(57) Sintic, P. J.; E, W.; Ou, Z.; Shao, J.; McDonald, J. A.; Cai, Z.-L.; Kadish, K. M.; Crossley, M. J.; Reimers, J. R. Control of the site and potential of reduction and oxidation processes in π-expanded quinoxalinoporphyrins. *Phys. Chem. Chem. Phys.* **2008**, *10*, 268−280.
(58) Kadish, K. M.; Rhodes, R. K. Reactions of metalloporphyrin. pi. radicals. 2. Thin-layer spectroelectrochemistry of zinc tetraphenylporphyrin cation radicals and dications in the presence of nitrogenous bases. *Inorg. Chem.* **1981**, *20*, 2961−2966.
(59) Kadish, K. M.; Cornillon, J. L.; Cocolios, P.; Tabard, A.; Guilard, R. Electrochemistry and spectroelectrochemistry in indium(III) porphyrins. Reactions of five-coordinate ionic complexes. *Inorg. Chem.* **1985**, *24*, 3645−3649.
(60) Brueckner, C.; Chaudhri, N.; Nevonen, D. E.; Bhattacharya, S.; Graf, A.; Kaesmann, E.; Li, R.; Guberman-Pfeffer, M. J.; Mani, T.; Nimthong-Roldan, A.; et al. Structural and Photophysical Characterization of All Five Constitutional Isomers of the Octaethyl-β,β'-dioxobacterio- and -isobacteriochlorin Series. *Chem.—Eur. J.* **2021**, *27*, 16189−16203.
(61) Gao, S.; Li, C.; Baryshnikov, G.; Agren, H.; Li, Q.; Xie, Y. Stable thiophene-embedded N-confused homoporphyrins: Partial conjugation, fusion and fluoride binding. *Dyes Pigm.* **2021**, *194*, 109612.
(62) Koga, D.; Ono, T.; Shinjo, H.; Hisaeda, Y. J. Hydrogen Bond Engineering Visualized by Picometer-Level Distortion of Planar Porphyrin Isomers. *Phys. Chem. Lett.* **2021**, *12*, 10429−10436.
(63) Listkowski, A.; Masiera, N.; Kijak, M.ł; Luboradzki, R.; Lesniewska, B.; Waluk, J. Waluk, Controlling Emissive Properties by Intramolecular Hydrogen Bonds: Alkyl and Aryl meso-Substituted Porphycenes. J. *Chem.—Eur. J.* **2021**, *27*, 6324−6333.
(64) Nemykin, V. N.; Sabin, J. R. Profiling Energetics and Spectroscopic Signatures in Prototropic Tautomers of Asymmetric Phthalocyanine Analogues. *J. Phys. Chem. A* **2012**, *116*, 7364−7371.
(65) Dyrda, G.; Broda, M. A.; Hnatejko, Z.; Pedzinski, T.; Slota, R. Adducts of free-base meso-tetraarylporphyrins with trihaloacetic acids: Structure and photostability. *J. Photochem. Photobiol., A* **2020**, *393*, 112445.

https://doi.org/10.1021/acsphyschemau.2c00023
ACS Phys. Chem Au 2022, 2, 468−481

(66) Tang, M.; Yang, Y.; Zhang, S.; Chen, J.; Zhang, J.; Zhou, Z.; Liu, Q. Electron Transfer and Geometric Conversion of Co−NO Moiety in Saddled Porphyrins: Implications for Trigger Role of Tetrapyrrole Distortion. *Inorg. Chem.* **2018**, *57*, 277−287.
(67) Roucan, M.; Flanagan, K. J.; O'Brien, J.; Senge, M. O. Nonplanar Porphyrins by N -Substitution: A Neglected Pathway. *Eur. J. Org. Chem.* **2018**, *2018*, 6432−6446.
(68) Grover, N.; Kumar, R.; Chaudhri, N.; Butcher, R.; Sankar, M. *β*-Heptasubstituted Porphyrins: Synthesis, Structural, Spectral, and Electrochemical Properties. *Eur. J. Inorg. Chem.* **2018**, *2018*, 3338−3343.
(69) Spyroulias, G. A.; Despotopoulos, A. P.; Raptopoulou, C. P.; Terzis, A.; de Montauzon, D.; Poilblanc, R.; Coutsolelos, A. G. Comparative Study of Structure-Properties Relationship for Novel *β*-Halogenated Lanthanide Porphyrins and Their Nickel and Free Bases Precursors, as a Function of Number and Nature of Halogens Atoms. *Inorg. Chem.* **2002**, *41*, 2648−2659.
(70) Jia, S.-L.; Jentzen, W.; Shang, M.; Song, X.-Z.; Ma, J.-G.; Scheidt, W. R.; Shelnutt, J. A. Axial Coordination and Conformational Heterogeneity of Nickel(II) Tetraphenylporphyrin Complexes with Nitrogenous Bases. *Inorg. Chem.* **1998**, *37*, 4402−4412.
(71) Song, X.-Z.; Jentzen, W.; Jaquinod, L.; Khoury, R. G.; Medforth, C. J.; Jia, S.-L.; Ma, J.-G.; Smith, K. M.; Shelnutt, J. A. Substituent-Induced Perturbation Symmetries and Distortions of meso-tert-Butylporphyrins. *Inorg. Chem.* **1998**, *37*, 2117−2128.
(72) Belosludov, R. V.; Nevonen, D.; Rhoda, H. M.; Sabin, J. R.; Nemykin, V. N. Simultaneous Prediction of the Energies of Qx and Qy Bands and Intramolecular Charge-Transfer Transitions in Benzoannulated and Non-Peripherally Substituted Metal-Free Phthalocyanines and Their Analogues: No Standard TDDFT Silver Bullet Yet. *J. Phys. Chem. A* **2019**, *123*, 132−152.
(73) Mack, J.; Bunya, M.; Shimizu, Y.; Uoyama, H.; Komobuchi, N.; Okujima, T.; Uno, H.; Ito, S.; Stillman, M. J.; Ono, N.; Kobayashi, N. Application of MCD Spectroscopy and TD-DFT to Nonplanar Core-Modified Tetrabenzoporphyrins: Effect of Reduced Symmetry on Nonplanar Porphyrinoids. *Chem.—Eur. J.* **2008**, *14*, 5001−5020.
(74) Mack, J.; Stillman, M. J.; Kobayashi, N. Application of MCD spectroscopy to porphyrinoids. *Coord. Chem. Rev.* **2007**, *251*, 429−453.
(75) Mack, J.; Asano, Y.; Kobayashi, N.; Stillman, M. J. Application of MCD Spectroscopy and TD−DFT to a Highly Non-Planar Porphyrinoid Ring System. New Insights on Red−Shifted Porphyrinoid Spectral Bands. *J. Am. Chem. Soc.* **2005**, *127*, 17697−17711.
(76) Martynov, A. G.; Mack, J.; May, A. K.; Nyokong, T.; Gorbunova, Y. G.; Tsivadze, A. Y. Methodological Survey of Simplified TD-DFT Methods for Fast and Accurate Interpretation of UV−Vis−NIR Spectra of Phthalocyanines. *ACS Omega* **2019**, *4*, 7265−7284.
(77) Nemykin, V. N.; Hadt, R. G.; Belosludov, R. V.; Mizuseki, H.; Kawazoe, Y. Influence of Molecular Geometry, Exchange-Correlation Functional, and Solvent Effects in the Modeling of Vertical Excitation Energies in Phthalocyanines Using Time-Dependent Density Functional Theory (TDDFT) and Polarized Continuum Model TDDFT Methods: Can Modern Computational Chemistry Methods Explain Experimental Controversies? *J. Phys. Chem. A* **2007**, *111*, 12901−12913.

https://doi.org/10.1021/acsphyschemau.2c00023
ACS Phys. Chem Au 2022, 2, 468−481